Journal of Ambient Intelligence and Humanized Computing
https://doi.org/10.1007/s12652-022-03787-z

ORIGINAL RESEARCH

Hybrid convolutional neural network based segmentation of visceral and subcutaneous adipose tissue from abdominal magnetic resonance images

B. Sudha Devi[1] · **D. S. Misbha**[2]

Received: 19 October 2021 / Accepted: 25 February 2022

Abstract
Globally, obesity is on the rise. According to the world health organization over 300 million people in the world are obese. India is the third most obese country in the world. It is noteworthy that 30 million people are obese in India alone. If a person's body weight is 20% higher than normal, it means he is obese. People who are obese are at a much higher risk of developing many severe ailments than normal or healthy weight. Visceral adipose tissue (VAT) quantity and subcutaneous adipose tissue (SAT) (volume) is generally higher for those with obesity. Hence, developing a computer vision-based fully automated visceral and subcutaneous adipose tissue segmentation and quantification system is an urgent research problem. This can be very useful for physicians to predict a wide variety of highly absurd diseases earlier. In this research, a fully automated hybrid deep learning framework has been developed to optimize VAT and SAT segmentation from non-contrast abdominal MRI images. The texture layer is included in traditional convolutional neural network architecture for CNN hybridization to improve classification performance and reduce computational cost. This will reduce the unwanted iteration which takes place during feature learning, which further reduces the computational complexity and unwanted memory requirements of the traditional CNN model. Back-propagation algorithms are generally used to train CNN, which unnecessarily consumes a lot of time to train the model. This research has developed an improved back-propagation algorithm to reduce unwanted training time. The performance of the proposed method is evaluated using mean absolute error (MAE), mean square error (MSE), and root mean square error (RMSE). Experimental results make it clear that the performance of the proposed VAT segmentation system is better than state-of-the-art methods.

Keywords Adipose tissue segmentation · Computer vision · Computed tomography · Magnetic resonance imaging · Obesity · Segmentation · CNN

1 Introduction

Generally, a body mass index (BMI) of ≥ 30 is considered a significant health problem. Obesity is a growing problem these days (Arthur et al. 2011). Obesity usually refers to the excess of body fat in the human body. Obesity is a major health concern caused by unhealthy eating behaviours and does not burn off the energy through exercise, which is closely related to many diseases. VAT and SAT, also known as belly fat, is the most dangerous fat stored in the human abdomen and around the most important organs such as the stomach, kidneys, intestines, liver, pancreas, and heart (Yan et al. 2015; Corbeil et al. 2001). Excess Adipose Tissues (VAT and SAT) increases the risk for heart disease, diabetes, arterial disease, stroke, and some cancers (Ding et al. 2014, 2015).

Whole-body body fat is the primary indicator of obesity. Many calculation methods and clinical instruments are now available to measure obesity, including bod pod, Dual-energy X-ray Absorptiometry (DXA), and Biomedical Impedance Analysis (BIA) (Norlén et al. 2016; Shen

✉ B. Sudha Devi
sudhanixen@gmail.com

D. S. Misbha
misbhasatheesh4@gmail.com

[1] Department of Computer Science, Nesamony Memorial Christian College Affiliated to Manonmaniam Sundaranar University, Tirunelveli, Tamilnadu 627012, India

[2] Department of Computer Applications, Nesamony Memorial Christian College Affiliated to Manonmaniam Sundaranar University, Tirunelveli, Tamilnadu 627012, India

Published online: 22 April 2022

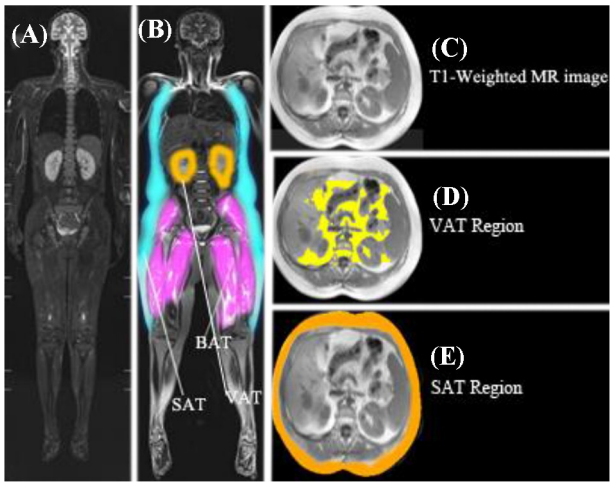

Fig. 1 Illustrates MRI images of people with two different BMIs. **A** An MRI scan image of a healthier person is displayed. **B** Shows an MRI scan image of a person with a BMI > 30. **D**, **E** An illustration of different types of adipose tissues in abdominal MRI imaging. **C** Shows the abdominal MRI image of a fatty man

et al. 2019). However, these methods are not capable of properly quantising VAT deposited in the abdominal region and abdominal organs (Franke 1993). The imaging process of VAT and SAT deposited in the abdominal region and abdominal organs is effectively done by computed tomography (CT) or magnetic resonance imaging (MRI) (Kullberg 2010; Ibrahim et al. 2019). Figure 1 depicts a whole-body MRI of two individuals with significantly varied BMIs.

SAT and VAT segmentation from abdominal MR images helps physicians to predict many diseases in a very earlier stage (Hussein 2017). Medical researchers and academic researchers have conducted various studies to classify and quantify these two different types of tissues. However, computerized isolation of VAT and SAT in MRI is a very complex and time-consuming task due to the similar intensity characteristics of the images. Radiologists generally use morphological based image processing tools to segregate SAT and VAT separately. In this process, more than 50% of the process is done manually (Sussman et al. 2010; Wuerslin et al. 2009). Only an experienced radiologist can do this segmentation and quantification moderately better, and this is a time-consuming task. The sole aim of this proposed research is to develop an accurate and fully automated adipose tissue segmentation and quantization system to predict life-threatening diseases earlier.

The convolutional neural network (CNN) is one of the most important classes of deep learning (Lu et al. 2019; Roy et al. 2020). Recently, CNN has provided remarkable outcomes in medical image processing due to its outstanding performances, especially for identifying and classifying prostate and brain cancers, analysis of CT lung images, breasts and others. However, developing an excellent and more reliable CNN model requires a large amount of computational resources (Graphical Processing Units (GPU) and storage devices) (Song 2016). This proposed research includes an automatic texture features extraction layer with traditional CNN architecture. The novel texture features extraction layer is included next to the convolution process. The back propagation algorithm is generally used to train the CNN model. However, the traditional back propagation algorithm takes longer training because it requires lower learning rates for stable learning (Mizutani 1994; Khellal et al. 2018). In this article, an Exponential-based Learning Rate Schedule (EBLRS) and momentum coefficient have been used to optimize the traditional back propagation algorithm so that global minima can be achieved in a very short time. Further, the texture features are extracted from the MR images and trained by improved forward and backward propagation methods. Finally, proven experimentally, the texture-based CNN and innovative training model is superior in accuracy and performance over traditional methods. The main contributions of this work are summarized as follows:

The soul aim of this research are:

- In this article, CNN's feature extraction process is made light-weighting by the texture feature extraction layer, and high accuracy can be achieved with minimal features from abdominal MRI images.
- The traditional BP algorithm has been optimized with the Exponential-based Learning Rate Schedule (EBLRS) and momentum coefficient to improve the CNN-based VAT segmentation model's training efficiency.
- Finally, the proposed CNN model has been implemented and comparatively analyzed with the traditional methods. Experimental results make it clear that it has achieved up to 96% accuracy.

This research is organized as follows: In Sect. 2, already proposed VAT and SAT segmentation methods and algorithms are reviewed in detail. Then, the proposed CNN based VAT and SAT segmentation system is discussed and explained in Sect. 3. Next, experiments and results are presented in Sect. 4. Finally, Sect. 5 presents the conclusion of this work.

2 Related works

This section reviews the state-of-the-art VAT and SAT segmentation methods in detail.

Kucybała et al. (2020) established a graph-based system for automating the segmentation of visceral adipose tissue from

three-dimensional abdominal computed tomography images. The authors employ three image processing modules to separate SAT and VAT: CT image thresholding, body area recognition, and SAT and VAT separation. However, this approach does not automatically adjust to obese patients, as the adjacent regional and VAT cavities cause a loss in the segmentation.

Hussein et al. (2016) created a computer-aided design (CAD) system for isolating white and brown adipose tissues in positron emission tomography and computed tomography images. There are two components in this vision-based adipose tissue segmentation system. The first module uses unsupervised learning to differentiate white adipose tissue (WAT) and its two subcategories. Then, the volume of WAT is calculated using a context-driven label fusion technique. The second module employs a co-segmentation approach to segment and quantifies brown adipose tissue. Finally, the probabilistic distance metric distinguishes between WAT and BAT. Nevertheless, this is a semi-automatic system.

Masoudi et al. (2020) developed a segmentation method for separating adipose tissue in abdominal MR images using deep learning algorithms and cross-modality adaptation. To ease fat separation, this method use a cycle generative adversarial network rather than supervised labelling. The first module of this approach is called C-GAN, and it converts MR images to its equant CT format. VAT and SAT were separated using two U-Net models. Despite the fact that the system is automated, MR images are transformed into CT scans, resulting in the loss of many critical features. This unavoidably casts doubt on the segmentation's efficacy.

Shen et al. (2016) proposed a method for segmenting SAT and VAT using IDEAL-IQ sequences. In order to extract the SAT pattern, a deep neural network was trained first. The inside and outer margins of SAT are segmented in fat images and also in the peritoneal cavity contour in the first phase. The VAT is then clustered using the AFK-MC2 (Assumption-Free K-Means++ with a Markov chain Monte Carlo) technique. The dataset used was obtained from 75 patients, and it attained an accuracy of between 96 and 97%.

Dabiri et al. (2020) developed a model for automatically recognising and segmenting skeletal muscle (SM), subcutaneous adipose tissue (SAT), visceral adipose tissue (VAT), and intramuscular adipose tissue from a CT image (IMAT). It consists of a localization network trained on over 12,000 pictures for the L3 axial slice and a fully convolutional classifier. Following that, a convolutional neural network with encoder-decoder architecture is used for segmentation. It achieved a mean Jaccard score of 97% for segmentation of SM and VAT tissues on 1327 images and 98% and 83% for segmentation of SAT and IMAT tissues on the same images. Additionally, a mean slice error of 0.872 was reported for L3 slice localisation using 1748 CT scan volumes.

Koitka et al. (2020), developed a fully automated biomarker that is reproducible and quantitative 3D volumetry of human tissue composition in standard CT exams of the abdomen. It was trained with 751 CTs and tested with 186 CTs. Multi-resolution U-Net 3D neural networks were employed for segmentation. The Hounsfield unit did the classification of adipose tissue or muscle. The correlation coefficients were obtained to be more than 99%. The data was observed in five levels. One of the major drawbacks of the used dataset is slice thickness which is 5 mm, and the dissimilarity of visceral fat and fat in organs. The output of segmentation could be post-processed through masking the abdominal cavity.

Estrada et al. (2019) proposed a method called FatSegNet to recognize, segment and measure the visceral and sub-cutaneous adipose tissue, in the abdominal region on Dixon MRI scans. It is a three-step process. In the first step, localization of the abdominal area is done using Dense Fully Convolutional Networks (CDFNet). Next, the adipose tissue is segmented in three different ways by individual CDFNets. It is validated by estimating segmentation accuracy (sixfold cross-validation), depending on the test and averaging randomly selected manually re-edited cases, and duplication of the effect of age and sex.

Ackermans et al. (2021) recommended a computerized multi-atlas method for segmentation of abdominal organs and examination of regional adipose tissue on water-fat MRI data. SAT and VAT were evaluated using an automatic algorithm that comprised of morphological operations and a multi-atlas-based segmentation method. MRI datasets were used for testing. Pre-processing consisted of removal of background, water-fat swaps at the edge, abdominal skin etc., using morphological operations. The Multi-atlas approach was used for segmentation in which a newly available volume was fused with already available annotated image volumes, and then the resultant transform was used to carry out the annotations to the coordinate space. SAT and VAT were evaluated using an automatic algorithm that comprised of morphological operations and a multi-atlas-based segmentation method. MRI datasets were used for testing.

3 Methods

CNN delivers accurate segmentation results in most medical imaging. However, training the CNN model requires a lot of memory and a specialized graphical processing unit (GPU) (Ren 2020; Yuan et al. 2021). This proposed research effectively reduces the unnecessary computational costs incurred during CNN visceral adipose tissue segmentation. The overall architecture of the proposed VAT and SAT segmentation system from abdominal MRI images is visualized in Fig. 2. This method comprises three critical modules: MR image enhancement module, a novel CNN architecture for

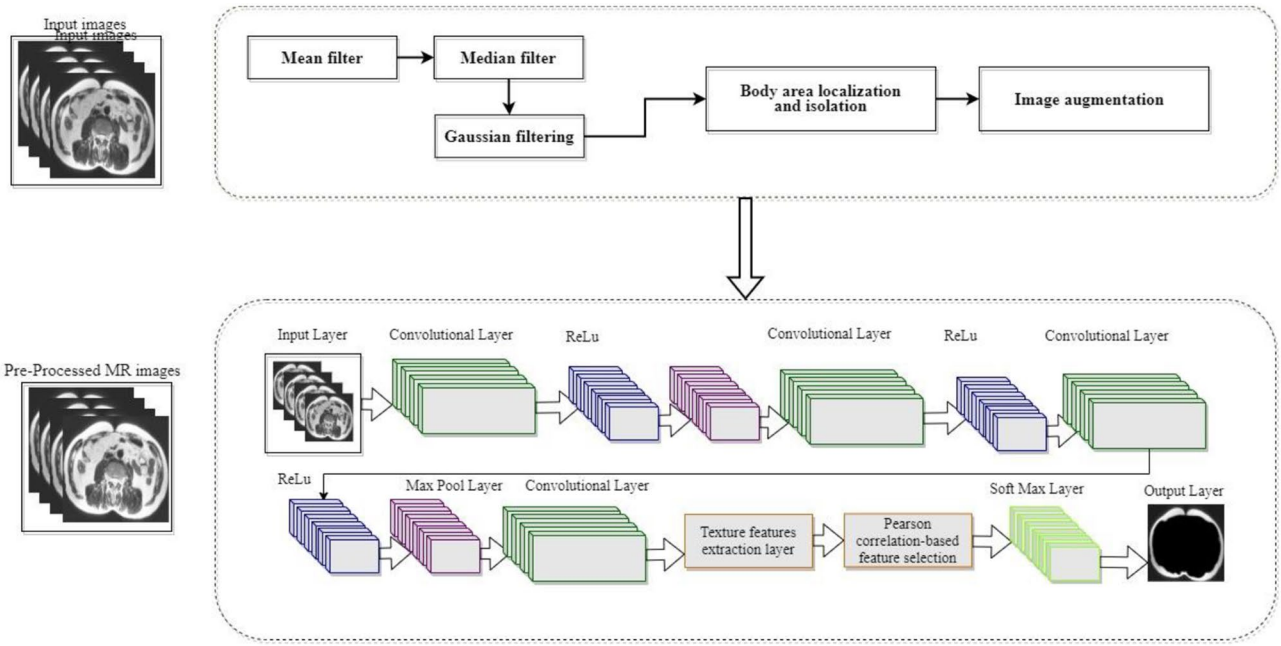

Fig. 2 Proposed VAT and SAT segmentation architecture from abdominal MR images, including a texture feature extraction (TFE) layer and a CNN architecture

extracting VAT and SAT features from MRI images and a Pearson correlation-based feature selection.

3.1 De-noising

Normally, deep learning-based image processing systems do not include a de-noising module. Although auto de-noising is a benefit of deep learning algorithms, training a model requires a significant amount of processing power and additional images. To effectively decrease this unwanted computational power caused by a large amount of training data, the proposed study adds a de-noising module before the CNN module. To denoise these abdominal MR images, three methods are being used: filtering techniques, body area localization and isolation, and image augmentation. Train the CNN model with minimal images and obtain an accurate VAT and SAT segmentation system using this denoising module.

3.1.1 Mean filter

The mean filter is a non-linear filtering technique that is frequently used to eliminate noise from an MR and other type's biomedical images. Using the mean filter, the mean value of the surrounding pixel values is used to replace the values of the center pixels in abdominal MR images. The average mean value of pixels in abdominal MR images is defined by Eq. (1).

$$\overline{P} = \frac{1}{n}P_1 + P_1 + P_2 + \cdots P_n. \tag{1}$$

3.1.2 Median filter

This study utilized the median filter to reduce salt and pepper noise from abdominal MR images. The median filtering technique calculates the median values of abdominal MR images by organizing the neighbor pixels in ascending order and finding the median among them. If the number of neighborhood pixels in abdominal MR images is odd, then it is defined by Eq. (2). The neighbor pixels in MR images are denoted by N_P.

$$M = Pixel\ Value\ of\left(\frac{(N_P+1)}{2}\right). \tag{2}$$

When the number of neighborhood pixel values in abdominal MR images is even, it is determined by Eq. (3).

$$M = \frac{Pixel\ Value\ of\left[\left(\frac{N_P}{2}\right) + \left(\frac{N_P}{2}+1\right)\right]}{2}. \tag{3}$$

3.1.3 Gaussian filtering

The speckle noise in MR images is caused by variations in the external or internal environment of the scanner. Due to Speckle Noise, deep learning systems struggle to locate edges, roughness, and lines in abdominal magnetic resonance images. Speckle noise will boost the VAT and SAT

segmentation method's false positive and false negative rates. The Gaussian filter was employed in this proposed work to efficiently minimize speckle noise in abdominal MR images.

3.1.4 Image augmentation

The dataset used for this study includes 512 abdomen MR images. In general, deep learning models perform worse when trained with fewer images and are more prone to model over fitting. To decrease over fitting and increase model accuracy, in this study, abdominal MR images are augmented. Using Python's deep learning library keras, abdominal MR images are rotated 90°, 180°, 360°, flipped horizontally, vertically, and zoomed.

3.1.5 Body area localization and isolation

To extract the backgrounds of MRI images, numerous techniques are available. The Otsu segmentation approach was employed in this study to isolate body region from a background in abdominal MR images. It categorizes MR images into two classes: foreground and background. The foreground class contains pixels from the body region, whereas the background class contains pixels from the image's dark region. A morphological closing operation is included to separate the foreground and background classes.

3.2 CNN architecture

Convolutional Neural Net (CNN) or ConvNet is a class of deep learning (Jiang et al. 2019). CNN is mainly used for image analysis in digital imaging. Its primary purpose is to efficiently extract beneficial information from images without the use of pre-processing and feature extraction. A CNN model is made up of different types of computing layers: the convolutional layer, the pooling layer, the fully connected layer and the Softmax layers (Jiang et al. 2019; Cao 2019). Figure 3 shows the general structure of CNN. The convolution layer is an essential component of CNN. The important purpose of the convolution layer is to extract the vital features from the input image. This convolution operation is done by using a small matrix. This matrix is called kernel or filter (Peng 2020). The kernel size varies depending on the input image, i.e. 3×3, 5×5, and others. The output obtained during the convolution process is called the feature map.

The next most important function of CNN is pooling which is applied next to the convolution operation. Pooling mainly provides down sampling operation to CNN which efficiently reduces the dimension of the feature maps. There are two main types of pooling used in CNN: Max pooling and average pooling. The highest values are selected from the feature map by Max pooling which is given in Fig. 3. The average value in the feature map is selected by the average pooling which is given in Fig. 4.

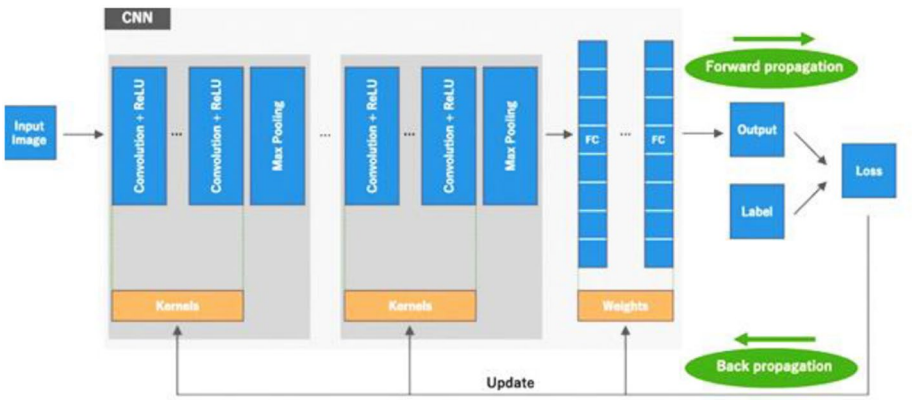

Fig. 3 The general architecture of traditional CNN

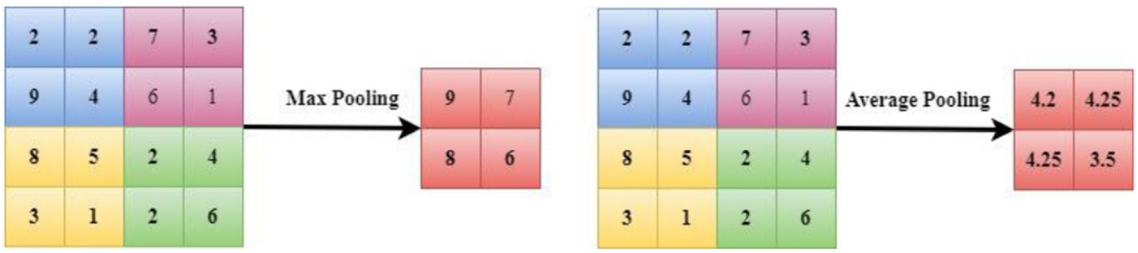

Fig. 4 Max-pooling and min-pooling process

This proposed CNN architecture has four convolutional layers. All convolutional process is followed by normalization and pooling operations. The newly introduced Texture Feature Extraction (TFE) layer is placed next to the final convolution layer. The most essential texture features collected from this layer are transferred to the fully connected layer. It is converted into a one-dimensional array. The layer details of this proposed model are explained in Table 1.

3.3 Texture feature extraction layer

In computer vision, feature extraction is the process of extracting higher-level quantitative information from images, such as image shape, color, texture, contrast, and brightness, to train or test machine learning or deep learning models. The extraction of texture features from MRI images is critical for training machine learning or deep learning models for MRI image analysis. Optimal Texture feature extraction approaches significantly increase the classification or segmentation accuracy of computer vision-based artificial intelligence (AI) algorithms. Moreover, effective feature extraction algorithms limit the number of computational resources required for AI model training.

The proposed research extracts different types of texture features from MR images. It is easy to find out if there are any changes in the images with texture feature extraction. The feature selection method is employed in this proposed method to extract the most optimal texture feature from MR images. These outstanding texture features significantly boost segmentation accuracy and lower the deep learning models' computing cost. The following formulas determine the important texture features of this research: autocorrelation, contrast, correlation, energy, dissimilarity, entropy, homogeneity, variance and cluster shade.

$$\text{Autocorrelation} = \sum_{i}\sum_{j}(i,\ j)p(i,\ j) \tag{4}$$

$$Contrast = \sum_{n=0}^{N_e-1} n^2 \sum_{n=i}^{N_e}\sum_{n=j}^{N_e}\{p(i,\ j)\} \tag{5}$$

$$Correlation = \frac{\sum_i \sum_j (i,\ j)p(i,\ j) - \mu_x\mu_y}{\sigma_x\sigma_y} \tag{6}$$

$$Energy = \sum_{i}\sum_{j} p(i,\ j) \tag{7}$$

$$Dissimilarity = \sum_{i}\sum_{j} |i-j| * p(i,\ j) \tag{8}$$

$$Entropy = \sum_{i}\sum_{j} p(i,\ j)\log(p(i,\ j)) \tag{9}$$

$$Homogeneity = \sum_{i}\sum_{j} \frac{1}{1+(i-j)^2} p(i,\ j) \tag{10}$$

$$Variance = \sum_{i}\sum_{j} (i-\mu)^2 p(i,\ j) \tag{11}$$

$$Cluster\ shade = \sum_{i}\sum_{j} (i+j-\mu_x-\mu_y)^2 p(i,\ j) \tag{12}$$

The extracted features are stored in the F vector. This is specified by formula (13).

$$\vec{F} = \left[A_c,\ C_t,\ C,\ E,\ D_s,\ E_n,\ H,\ V,\ C_s\right] \tag{13}$$

In general, advanced feature selection approaches increase deep learning-based classification or segmentation efficiency. However, if the feature selection approach is not excellent, the deep learning model is trained with weak features, resulting in a low dice score for the segmentation system (Yuan et al. 2021; Chang et al. 2016). The low dice score of medical segmentation has serious

Table 1 Layer-wise details of proposed CNN for VAT segmentation

Layer	Input size of CNN	Kernel size of CNN	Stride size of CNN	Padding size of CNN	Output size
Conv1	64×64×1	5×5	[1 1]	[1 1 1 1]	64×64×16
Pool1	64×64×16	2×2	[2 2]	[1 1 1 1]	32×32×16
Conv2	31×31×16	5×5	[1 1]	[1 1 1 1]	30×30×32
Pool2	30×30×32	2×2	[2 2]	[1 1 1 1]	16×16×32
Conv3	16×16×32	3×3	[1 1]	[1 1 1 1]	16×16×64
Pool3	16×16×32	2×2	[2 2]	[1 1 1 1]	16×16×32
Conv4	8×8×32	3×3	[1 1]	[1 1 1 1]	16×16×64
FC1	128×1	NA	NA	NA	1024×1
FC2	1024×1	NA	NA	NA	2×1

consequences for patients. Hence, medical image processing must employ a highly reliable feature selection technique. The extracted features are specified in the following format.

$$F = \begin{bmatrix} \overrightarrow{f1} \\ \overrightarrow{f2} \\ \overrightarrow{f3} \\ . \\ . \\ \overrightarrow{fn} \end{bmatrix}, \quad C = \begin{bmatrix} c1 \\ c2 \\ c3 \\ . \\ . \\ cm \end{bmatrix} \tag{14}$$

In the above formula, F has n features vectors extracted using the texture feature extraction method, and C has m class pixels. The values of n and m depend on the structure of the MR images. Formula (15) examines the correlation between F and C.

$$Cor_{fc} = \frac{\sum(F_i - \overline{F})(C_i - \overline{C})}{\sqrt{\sum(F_i - \overline{F})^2 \sum(C_i - \overline{C})^2}}. \tag{15}$$

In the above equation, $\overline{F}$ signifies the observed mean value of the feature map, and $\overline{C}$ denotes the ground truth average value. If the correlation between the features and the ground truth of the MR image is high, formula (15) returns values between 1 and 0.7. To select the strongest features in MR images, the correlation value of the features is 0.7 or higher is chosen. Algorithm 1 describes the recommended high correlated texture feature extraction method's process flow and pseudo code.

Algorithm 1: Texture Feature Extraction Algorithm

Input: $(T_{f1,}T_{f2,}T_{f3,}\_\_\_\_\_T_{fn})$
Output: F_{Best}
Begin
For $i = 1$ *to n texture features*
  $Cor_{fc} = (T_{fi})$// *using formula 14*
  Set τ*=0.7 //* τ *is the threshold value*
  If $(Cor_{fc} < \tau)$
    There is no significant correlation
  Else
    $F_{List} \leftarrow Add(T_{fi})$
  End If
End For
$F_{Best} \leftarrow F_{List}$
Return F_{Best}

3.4 Fine tuning the learning parameters

Learning parameters and learning values play a significant role in CNN. Training efficiency varies depending on the fine-tuning of CNN's important parameters such as dropout rate, learn rate, and decay rate. Even the best CNN model may fail to give an actual result if the important learning parameters are not fine-tuned. Deep learning models are frequently trained using the back propagation (BP) algorithm. It will keep updating the learning parameter values in the forward and backward directions until it reaches the global minima. Simultaneously, as the data set size grows, it takes many hours to reach the global minima. As a result, training a deep learning model necessitates a significant amount of processing power and time. The primary aim of this paper is to save unnecessary computing costs and attain global minima more efficiently. In order to improve back propagation, a hybrid learning parameters tuning approach based on the Exponential-Based Learning Rate Schedule (EBLRS) and the momentum coefficient is introduced in this paper. The weight updating procedure in existing back propagation is based on Eq. (16).

$$w_{(t+1)} = w_t - \eta \frac{d(E)}{d(w_1)} \tag{16}$$

$w_{(t+1)}$ signifies the CNN model's weight increase, η denotes the CNN learning rate, and $d(E)$ denotes the total error that arises when training the CNN model. The momentum coefficient is utilized here to improve the BP algorithm's training efficiency. The momentum coefficient is defined by the equation below. The momentum coefficient is used to update the training weight, and α indicates momentum coefficient

$$\Delta w_t = \alpha \Delta w_{(t-1)} + \eta \frac{d(E)}{d(w_1)}. \tag{17}$$

The training efficiency is determined by the learning rate and other learning parameters. If it is low, it will take longer to reach the global minima, whereas if it is high, oscillation is possible. The following equation, inspired by the Exponential-Based Learning Rate Schedule (EBLRS) algorithm, is used in this work to determine the ideal learning rate. Where η_0 denotes the initial learning rate, d denotes the decay rate, and n denotes the iteration step.

$$\eta_n = \eta_0 e^{-dn}. \tag{18}$$

The squared error function calculates the error of each output. To get the overall error, add the error values using

Eq. (19), where t_v is the target value and o_v is the observed value.

$$E_t = \sum \frac{1}{2}(t_v - o_v)^2. \tag{19}$$

Algorithm 2 describes the process for optimizing learning rate and weight updating procedure for the proposed CNN model.

3.5 Train the CNN model

Adam optimizer is used for training the input images and the related feature maps for segmentation. Soft-max over the final feature map and the Dice loss function are combined to update the weighing values. Soft-max is defined as,

$$\mathrm{S_k}\ (L) = \exp(m_k(L))/\left(\sum_{k'=1}^{k} \exp(m_{k'}(L))\right), \tag{20}$$

where $m_k(L)$ indicates the activation at the pixel position L in feature channel k. $\mathrm{S_k}$(L) is the maximum-function approximation. The Dice loss function is given by:

$$D(\theta) = \frac{2\sum_{L\in\omega} p_{\theta(L)P(L)}}{\sum_{L\in\omega} p(L)^2 + \sum_{L\in\omega} p_\theta(L)^2} \tag{21}$$

where p(L) represents the pixel label and θ represents the feature map.

Algorithm 2 : Training optimization and weight updating procedure for proposed CNN

1. *Initialize the CNN models network biases values and weights.*
2. *CNN's weight normalization using* $\omega = \frac{x-m}{x_{max}-x_{min}}$ // *where ω is the network weight, m is the mean value of the CNN's input,* x_{max} *is the maximum value of the CNN's input and* x_{min} *is the minimum value of the CNN's input.*
3. *Update the training weight momentum coefficient* ($\Delta w_t = \alpha \Delta w_{(t-1)} + \eta \frac{d(E)}{d(w_1)}$).
4. *Set the optimal learning rate using the Exponential-Based Learning Rate Schedule (EBLRS) algorithm* ($\eta_n = \eta_0 e^{-dn}$).
5. *Determine the model's prediction error using* ($\eta_n = \eta_0 e^{-dn}$)
6. *Repeat steps 3 and 4 until reach the minimal error rate.*

4 Results

4.1 System setup

To implement the suggested VAT and SAT segmentation system, a workstation equipped with a 10th Generation Intel Core i7-10750H (12 MB Cache, up to 5.0 GHz, six cores), 4 GB NVIDIA GEFORCE GTX, 2 × 8 GB DDR3, and 512 GB M.2 PCIe NVMe Solid State Drive was employed. Its working model was constructed using Python 3.7, machine learning frameworks, Keras, TensorFlow, PyTorch, and Deep Learning libraries.

4.2 Dataset details

The developed CNN-based VAT and SAT segmentation algorithms are evaluated for training and computational efficiency using the most widely used data set, CHAOS (Combined (CT-MR) Healthy Abdominal Organ Segmentation). This data collection contains two types of scan images: abdominal magnetic resonance imaging (MR) and computed tomography (CT) (weighing T1 and T2). The ultimate aim of this data set is to separate the kidney, spleen, and liver from CT and MR images. Both forms of abdominal scan images are derived from a patient's DICOM images. To train and evaluate the proposed CNN model, 100 T1 weighted MRI slices are collected from each DICOM format image. Accordingly, 10,000 T1 MR slices are retrieved from 100 randomly selected DICOM images. All these images are in DICOM format so all these images are converted to JPG format and resized to 520 × 520 before the model is trained. To train the proposed VAT segmentation model, MR images are randomly selected from the data set. The K-Fold cross-validation approach is employed here to assess the training efficiency of the proposed CNN model in various combinations. This data set was large enough to train a CNN capable of accurately segmenting visceral fat. However, due to the complexity of visceral fat segmentation, a larger number of training images were necessary for successful training. In this study, data augmentation is used to compensate for the low amount of MR images by rotating them 90°, 180°, 360°, flipping them horizontally and vertically, and zooming them.

4.3 Evaluation metrics

Three important error evaluation methods have been used to measure the error rate of the proposed CNN model: Mean Absolute Error (MAE), Mean Square Error (MSE), and Root Mean Square Error (RMSE) (Kitil et al. 2018; Ramchoun et al. 2016). If the value of (MAE), (MSE),

and (RMSE) is low, then the performance of the presented CNN model is high. These error evaluation techniques are calculated by Eqs. (22, 23, and 24).

MAE returns the error statistics of the N samples. It averages the distances between the estimated and predicted data for N samples. Where $\widehat{yi}$ is the estimated value, and yi is the observed value.

$$MAE = \frac{1}{N}\sum_{i=1}^{N}\left|yi - \widehat{yi}\right|. \tag{22}$$

MSE is defined as the average square difference between observed prediction value and predicted results.

$$MSE = \frac{1}{N}\sum_{i=1}^{N}\left|yi - \widehat{yi}\right|^2. \tag{23}$$

The RMSE returns the standard deviation of the difference between the observed data and estimation data of the VAT segmentation model.

$$RSME = \sqrt{\frac{1}{N}\sum_{i=1}^{N}\left|yi - \widehat{yi}\right|^2}. \tag{24}$$

Traditional BP algorithm and improved BP algorithm have been used for experimental analysis. The configuration of the experiment is given in Table 2. The data set is divided into three parts (training, validation and testing) in different combinations and experimented with several times.

Table 3 displays MAE values, Table 4 displays MSE values, and Table 5 displays RMSE values. Table 7 shows the computational time (CT) comparison of the proposed method and the traditional methods. The MAE, MSE, and RMSE values of the proposed model are close to 0, which shows the efficiency of the proposed method, whereas the MAE, MSE, and RMSE values of the traditional model are above 1. Table 6 confirms that the traditional method takes a higher computational cost than the proposed method. The comparative analysis of the experiment results is shown in Figs. 5, 6, 7, 8. Comparative analysis shows the effect of the MAE, MSE, and RMSE (Figs. 5, 6, 7), CNN-Momentum-EBLRS model performs significantly better than the

Table 2 Control parameters of the present CNN-Momentum-EBLRS model

Parameters	Configuration
Number of convolutions layers	4
Pooling layers	3
Activation function	ReLu
Optimizer	Adam
Learning algorithm	Momentum-EBLRS

Table 3 MAE values of proposed BP algorithm and traditional BP algorithm

Data set partition ratios	Traditional BP algorithm (MAE)	Presented BP algorithm (MAE)
70:20:10	1.344	0.926
70:15:15	1.060	0.863
70:25:5	1.351	0.841
80:10:10	0.956	0.861
80:15:5	0.901	0.771
80:5:15	0.979	0.887
90:5:5	0.821	0.886
85:05:10	0.812	0.793
75:10:15	1.019	0.876
60:20:20	1.901	0.921
Average value	1.1144	0.8571

Table 4 MSE values of proposed BP algorithm and traditional BP algorithm

Data set partition ratios	Traditional BP algorithm (MSE)	Presented BP algorithm (MSE)
70:20:10	1.894	0.887
70:15:15	1.856	0.815
70:25:5	1.633	0.741
80:10:10	0.953	0.998
80:15:5	0.787	0.629
80:5:15	0.979	0.586
90:5:5	0.865	0.591
85:05:10	0.823	0.701
75:10:15	0.990	0.831
60:20:20	1.923	1.001
Average value	1.2702	0.778

Table 5 RMSE values of proposed BP algorithm and traditional BP algorithm

Data set partition ratios	Traditional BP algorithm (RMSE)	Presented BP algorithm (RMSE)
70:20:10	2.223	1.112
70:15:15	2.310	1.101
70:25:5	1.891	1.136
80:10:10	1.732	1.123
80:15:5	1.771	1.123
80:5:15	1.345	0.779
90:5:5	1.561	0.570
85:05:10	1.123	0.690
75:10:15	1.768	0.876
60:20:20	2.231	1.567
Average value	1.799	1.008

Table 6 Dice-score comparison results obtained using various combinations of K-Fold cross-validation

Dice score testing, K-Fold 70:20:10				Dice score testing, K-Fold 80:10:10		
Model	VAT	SAT	Average	VAT	SAT	Average
U-Net	0.936	0.927	0.932	0.958	0.966	0.962
MR U-Net 3D	0.949	0.945	0.947	0.962	0.964	0.963
VGG11	0.938	0.934	0.936	0.948	0.956	0.952
FatSegNet	0.955	0.958	0.957	0.974	0.968	0.971
DLNN	0.964	0.966	0.965	0.968	0.976	0.972
Proposed method	0.979	0.983	0.981	0.982	0.986	0.984

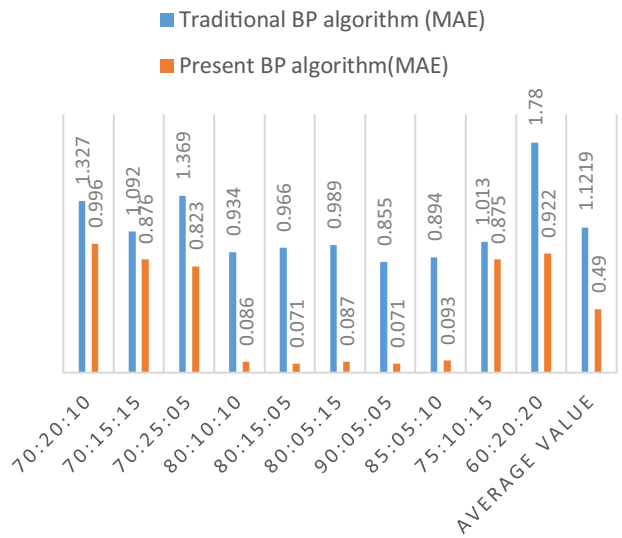

Fig. 5 Comparative analysis of MAE proposed CNN based VAT and SAT segmentation and the traditional methods

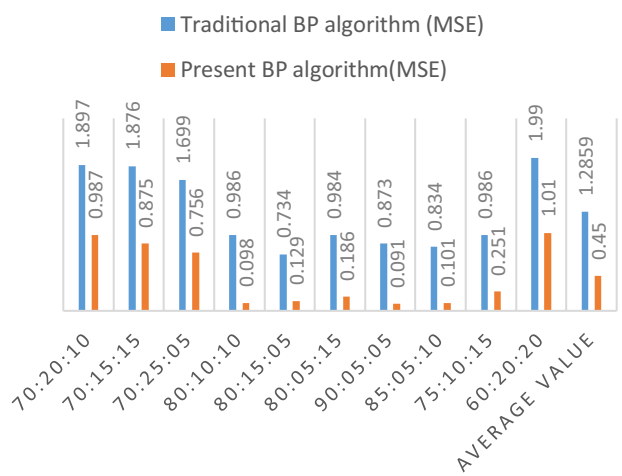

Fig. 6 Comparative analysis of MSE proposed CNN based VAT and SAT segmentation and the traditional methods

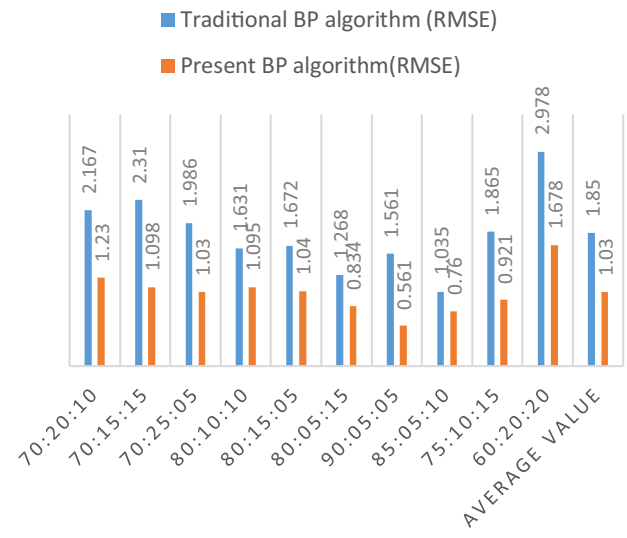

Fig. 7 Comparative analysis of MSE proposed CNN based VAT and SAT segmentation and the traditional methods

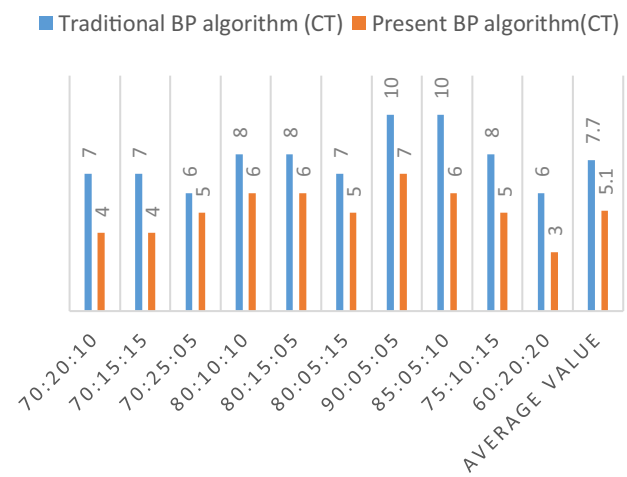

Fig. 8 Comparative analysis of MSE proposed CNN based VAT and SAT segmentation and the traditional methods

traditional BP-CNN in terms of MAE, MSE, and RMSE. Figure 8 shows the computational efficiency of the CNN-Momentum-EBLRS model. The proposed hybrid CNN based VAT segmentation model consumes an average of 7.7 min for training, validation, and testing. Experimental

results make it clear that better prediction results can be obtained by using a better learning rate and training method.

4.4 Experimental result

This section explains the experimental results obtained using the proposed CNN-based VAT segmentation method. Further, the specificity, sensitivity, and dice-score are used to determine the segmentation reliability of this automated VAT segmentation method. The segmentation efficiency of the proposed VAT segmentation approach is determined using Eqs. (25, 26, and 27).

$$Specificity = \frac{TN}{TN + FP} \tag{25}$$

$$Sensitivity = \frac{TP}{TP + FN} \tag{26}$$

$$Dice{-}score = \frac{2 \times TP}{FN + 2 \times TP + FP} \tag{27}$$

- True Positive VAT segmentation: True positive VAT segmentation happens whenever the suggested method correctly segments the visceral adipose tissue from abdominal MR images.
- True negative VAT segmentation: True negative VAT segmentation happens whenever the suggested method correctly segments the region lacking visceral adipose tissue from abdominal MR images.
- False positive VAT segmentation: False positive VAT segmentation happens whenever the proposed method mistakenly detects the appearance of visceral adipose tissue in abdominal MR images.
- False negative VAT segmentation: False negative VAT segmentation happens whenever the suggested approach

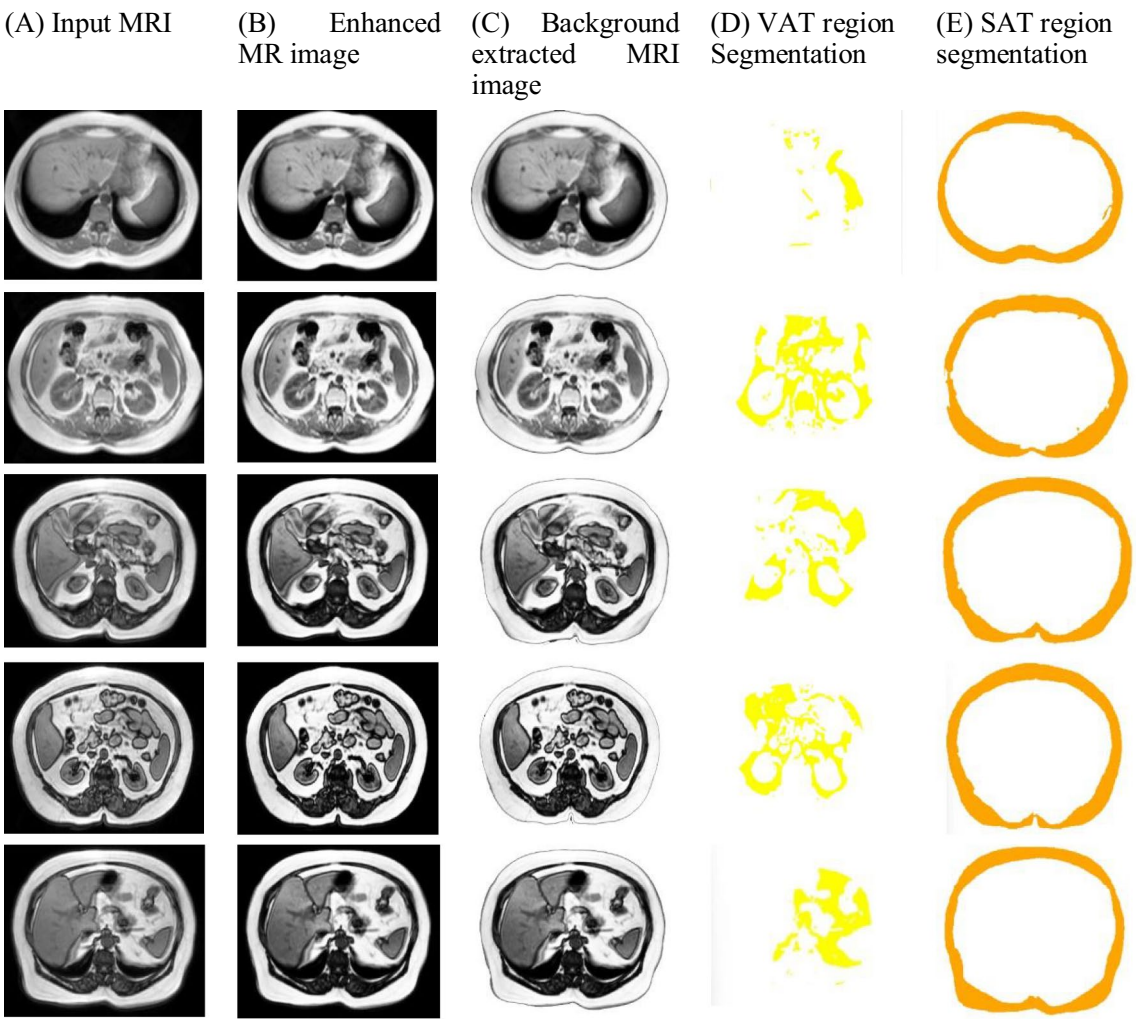

Fig. 9 The results of pre-processed MR images using the proposed CNN-based segmentation system and the results of segmentation of the extracted VAT and SAT regions

Table 7 Dice-score comparison results obtained using various combinations of K-Fold cross-validation

Dice score testing, K-Fold 75:20:5				Dice score testing, K-Fold 90:5:5		
Model	VAT	SAT	Average	VAT	SAT	Average
U-Net	0.942	0.936	0.939	0.938	0.936	0.937
MR U-Net 3D	0.936	0.940	0.938	0.939	0.933	0.936
VGG11	0.942	0.938	0.94	0.928	0.930	0.929
FatSegNet	0.945	0.939	0.942	0.948	0.963	0.956
DLNN	0.948	0.956	0.952	0.968	0.964	0.966
Proposed method	0.978	0.966	0.972	0.976	0.978	0.977

mistakenly suggests the lack of visceral adipose tissue in abdominal MR images.

In this study, Probabilistic Rand Index (PRI) is used as evaluation metric for the purpose of comparing two partitions such as VAT and non-VAT regions. The PRI ranges from 0 to 1, with 0 suggesting that the actual ground truth and the VAT segmentation result disagree on any pair of points and 1 indicating that the actual ground truth and the VAT segmentation result are exactly the same.

$$PRI = \frac{x_1 + x_2}{x_1 + x_2 + y_1 + y_2}. \tag{28}$$

The agreement pixel values between VAT segmentation and ground truth are x_1 and x_2, whereas the disagreement pixel values between VAT segmentation and ground truth are y_1 and y_2. The performance of the developed VAT and SAT segmentation method was compared to the recently established VAT segmentation methods such as U-Net, MR U-Net 3D, VGG11, FatSegNet, and DLNN. Figures 9A1–A5 shows T 1 weighted input abdominal MR images that have been preprocessed with a mean filter, a median filter, and a Gaussian filter. The filtered abdominal MR images are shown in Fig. 9B1–B5. The images that separate the body region from these preprocessed images by Otsu segmentation are displayed in Fig. 9C1–C5. The VAT region isolated by texture feature extraction and CNN is highlighted in the yellow shade which is displayed in Fig. 9D1–D5. Figure 9E1–E5 show the SAT region separated by the proposed method in an orange shade. To obtain reliable dice-score comparison results, K-Fold cross-validation is performed in various combinations, and its efficiency has been compared with recently established VAT segmentation algorithms. Tables 6 and 7 present the results of the dice-score comparison. The proposed VAT segmentation method has a higher Dice score than the existing methods.

4.5 Running time of the proposed algorithm

Running time is a critical performance measure for deep learning models. The performance of deep learning models is generally enhanced when the running duration is reduced. The suggested method's running time is classified into two parts: the time required to train a CNN model and the time required to isolate VAT and SAT from MR images. In general, the training of a deep learning model varies based on several critical aspects, including the CNN's network architecture, optimization techniques, and the hardware used to implement the model (GPU processor, RAM size, and CPU clock speed). To determine the proposed method's training time efficiency, the dynamically selected MR images are separated into five clusters and trained. Each cluster has a different number of images of 1000, 2000, 3000, 4000 and 5000 respectively. The developed method's training time was compared to the training times of recently established adipose tissue segmentation algorithms U-Net, MR U-Net 3D, VGG11, FatSegNet, and DLNN. Training time is measured in minutes.

The training duration comparison results for proposed and existing deep learning frameworks with their default parameters is shown in Fig. 10. As illustrated in Fig. 10, the VGG11 model requires the most time to train across all

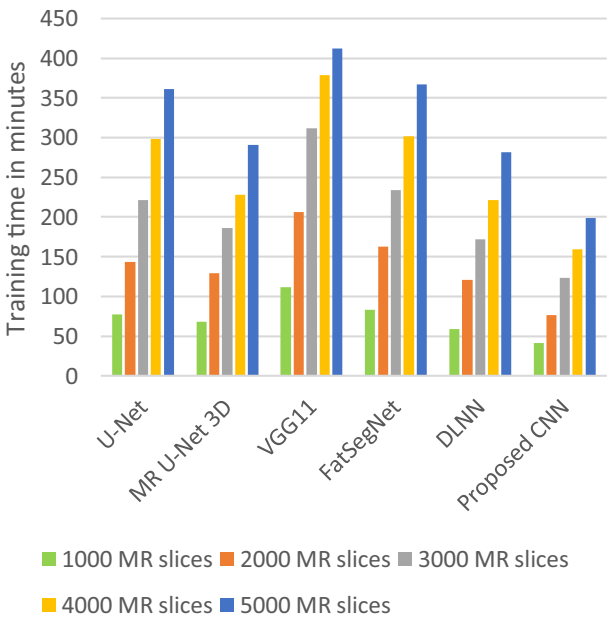

Fig. 10 The training time of proposed and existing deep learning frameworks using their default settings

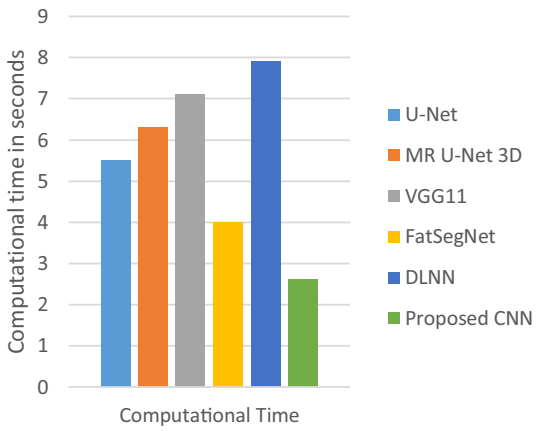

Fig. 11 The proposed method is compared with existing methods for extracting VAT and SAT from MR images in terms of computing time

datasets. The suggested model requires the least amount of training time across all datasets. Figure 11 compares the computing time required by the proposed method and existing methods for extracting VAT and SAT from MR images. To obtain accurate findings, MR images of five various sizes (200 KB, 400 KB, 600 KB, 800 KB, and 1000 KB) are used for each model, and the average computational time is used to determine the accurate comparison results. The time required for segmentation is measured in seconds.

According to Fig. 11, the DLNN model requires the maximum computational time (7.9 s) to segment the VAT and SAT regions from MR images, whereas the proposed model requires the least computational time (2.6 s).

4.6 Discussion

Obesity is one of the most prevalent health issues worldwide. Doctors can forecast a man's health based on the amount of fat stored in his abdominal region. As a result, separating the VAT and SAT regions from medical imaging technologies such as abdominal CT and MR images is a critical clinical research challenge. Although numerous approaches have been presented, an automated segmentation model for SAT and VAT that enhances efficiency and accuracy, particularly for MRI, has not yet been established.

The main objective of this proposed research is highly accurate VAT and SAT segmentation from abdominal MRI is accomplished in a highly efficient manner using CNN and a novel texture feature extraction layer. This proposed method has been developed using the deep learning method so that its robustness can be further enhanced with more abdominal MRI images. This study trained the suggested deep learning model using CHAOS (Combined (CT-MR) Healthy Abdominal Organ Segmentation). The benefits include an advance in automation, a more detailed VAT and SAT segmentation result, a model that requires little training data, and a model that requires minimal training and testing time.

The suggested architecture is composed of three modules, the central one of which is CNN, which automatically isolates VAT and SAT region from denoised images via feature extraction. The inclusion of texture feature extraction and correlated feature selection algorithms further improves segmentation dice scores. The texture feature extraction and correlated feature selection layers make the training process lighten thus unwanted computational power for model training is reduced multiple times. This is demonstrated by the results of its running time comparison.

Over fitting problems are common in Deep learning models due to the number of tuning parameters. The chances of over fitting problems are very high, especially when training deep learning models with fewer datasets. Image augmentation has been artificially created in this research to efficiently control this over-fitting problem. Further, the dropout rate, learn rate, and decay rate are dynamically fine-tuned to minimize the over fitting problem using momentum-EBLRS. Figure 12 depicts the proposed momentum-EBLRS regression curve. It is crucial to highlight that when trained using momentum-EBLRS, the CNN model performs substantially better than the other current approaches for VAT segmentation. Figure 12 clearly indicates the proposed CNN models overall (training, validation and test) predicted values that were closer to the 45 degree straight lines. Analyzing MR images and extracting VAT and SAT from them, the proposed CNN based model requires less than 3 s. The

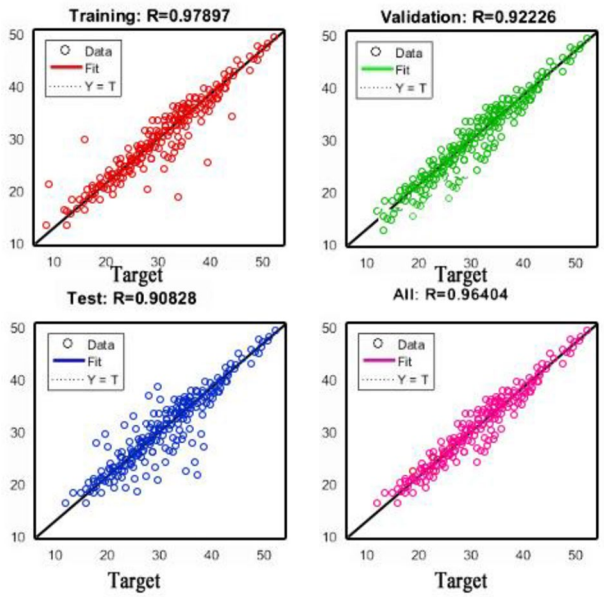

Fig. 12 Training efficiency regression plot of the proposed model while training with momentum-EBLRS

model training time for 5000 MR images was approximately 199 min on a system equipped with a 10th Generation Intel Core i7-10750H (12 MB Cache, up to 5.0 GHz, six cores), 4 GB NVIDIA GEFORCE GTX, and 2 × 8 GB DDR3. The most important aspects of this study are summarized here.

- This article demonstrates how the texture feature extraction layer helps lighten the weight of CNN's feature extraction procedure and how high accuracy can be obtained with few features from abdominal MRI scans.
- The conventional BP technique has been enhanced using the Exponential-based Learning Rate Schedule (EBLRS) and momentum coefficient in order to increase the training efficiency of the CNN-based VAT segmentation model.
- Finally, the suggested CNN model was applied and compared to more traditional approaches, with testing observations indicating that it attained up to 96% accuracy.

5 Conclusion

This research presents a method for automatically segmenting VAT and SAT in abdominal MR images. This study presented a Pearson correlation-based feature extraction approach for effectively extracting texture features in MR images. Moreover, a back propagation algorithm is used in traditional CNN to do model training. Therefore, it takes more time unnecessarily. In this study, a hybrid training method is proposed based on Momentum-EBLRS. Besides, this proposed method can greatly save doctors' excess time on visceral adipose tissue segmentation. Experimental results of state of the art CNN algorithms and the proposed CNN method make it clear that the results of the proposed method are very accurate, and the processing time is very short.

References

Ackermans LLGC et al (2021) Deep learning automated segmentation for muscle and adipose tissue from abdominal computed tomography in polytrauma patients. Sensors (Basel) 6:16–21

Arthur RM, Wang S, Trobaugh JW (2011) Changes in body-surface electrocardiograms from geometric remodeling with obesity. IEEE Trans Biomed Eng 58(6):1565–1573

Cao C (2019) An improved faster R-CNN for small object detection. IEEE Access 7:106838–106846

Chang X et al (2016) Compound rank-projections for bilinear analysis. IEEE Trans Neural Netw Learn Syst 27:1502–1513

Corbeil P et al (2001) Increased risk for falling associated with obesity: mathematical modeling of postural control. IEEE Trans Neural Syst Rehabil Eng 9:126–136

Dabiri S et al (2020) Deep learning method for localization and segmentation of abdominal CT. Comput Med Imaging Graph 85:101776

Ding X et al (2014) Automated epicardial fat volume quantification from non-contrast CT. International Society for Optics and Photonics, p 90340

Ding X et al (2015) Automated pericardium delineation and epicardial fat volume quantification from noncontrast CT. Med Phys 42:5015–5026

Estrada S et al (2019) FatSegNet: a fully automated deep learning pipeline for adipose tissue segmentation on abdominal dixon MRI. Magn Reson Med 83(4):6949410–6949410

Franke J (1993) System characterization of a highly integrated preclinical hybrid MPI-MRI scanner. IEEE Trans Med Imaging 35(9):1993–2004

Hussein S (2017) Automatic segmentation and quantification of white and brown adipose tissues from PET/CT scans. IEEE Trans Med Imaging 36(3):734–744

Hussein S et al (2016) Automatic segmentation and quantification of white and brown adipose tissues from PET/CT scans. IEEE Trans Med Imaging 36(3):6421081

Ibrahim SM et al (2019) A study on heart segmentation using deep learning algorithm for MRI scans. In: 2019 13th International conference on mathematics, actuarial science, pp 1–5

Jiang J et al (2019) Multi-spectral RGB-NIR image classification using double-channel CNN. IEEE Access 7:20607–20613

Khellal A, Ma H, Fei Q (2018) Convolutional neural network features comparison between back-propagation and extreme learning machine. 37th Chinese control conference (CCC), pp 9629–9634

Kitil AO, Kumar M, Gram-Lavale SI (2018) An IoT-based rain alerting and flood prediction using sensors and arduino for smart environment. Int J Pure Appl Math 118(24):1–12

Koitka S et al (2020) Fully automated body composition analysis in routine CT imaging using 3D semantic segmentation convolutional neural networks. Eur Radiol 31(4):7979624

Kucybała I et al (2020) A fast graph-based algorithm for automated segmentation of subcutaneous and visceral adipose tissue in 3D abdominal computed tomography images. Biocybern Biomed Eng 40(2):729–739

Kullberg J (2010) Whole-body MRI for analysis of body composition. In: 2010 IEEE international symposium on biomedical imaging: from nano to macro, pp 1065–1066

Lu L et al (2019) Integrating local CNN and global CNN for script identification in natural scene images. IEEE Access 7:52669–52679

Masoudi S et al (2020) Adipose tissue segmentation in unlabeled abdomen MRI using cross modality domain adaptation. Annu Int Conf IEEE Eng Med Biol Soc, p 33018306

Mizutani H (1994) The back propagation method for CNN. In: Proceedings of IEEE international symposium on circuits and systems—ISCAS '94, vol 6, pp 463–466

Norlén A et al (2016) Automatic pericardium segmentation and quantification of epicardial fat from computed tomography angiography. J Med Imaging 3(3):34003–034003

Peng Y (2020) FB-CNN: feature fusion-based bilinear CNN for classification of fruit fly image. IEEE Access 8:3987–3995

Ramchoun H et al (2016) Multilayer perceptron: architecture optimization and training. IJIMAI 4(1):26–30

Ren P (2020) A comprehensive survey of neural architecture search: challenges and solutions. ACM Comput Surv 37(4)

Roy SK et al (2020) HybridSN: exploring 3-D-2-D CNN feature hierarchy for hyperspectral image classification. IEEE Geosci Remote Sens Lett 17:277–281

Shen J et al (2016) Automatic segmentation of abdominal organs and adipose tissue compartments in water-fat MRI: application to weight-loss in obesity. Eur J Radiol 85(9):27501897

Shen N et al (2019) Automated and accurate quantification of subcutaneous and visceral adipose tissue from magnetic resonance imaging based on machine learning. Magn Reson Imaging 64:31004712

Song M (2016) Bridging the semantic gaps of GPU acceleration for scale-out CNN-based big data processing: think big, see small. In: 2016 International conference on parallel architecture and compilation techniques (PACT), pp 315–326

Sussman DL, Yao J, Summers RM (2010) Automated measurement and segmentation of abdominal adipose tissue in MRI. In: 2010 IEEE international symposium on biomedical imaging: from nano to macro, pp 936–939

Wuerslin C et al (2009) Automated segmentation of adipose tissue in magnetic resonance images of the whole body. In: IEEE nuclear science symposium conference record (NSS/MIC), pp 2476–2481

Yan L et al (2015) Capsule robot for obesity treatment with wireless powering and communication. IEEE Trans Ind Electron 62:1125–1133

Yuan D et al (2021) Self-supervised deep correlation tracking. IEEE Trans Image Process 30:976–985

Terms and Conditions

Springer Nature journal content, brought to you courtesy of Springer Nature Customer Service Center GmbH (“Springer Nature”).
Springer Nature supports a reasonable amount of sharing of research papers by authors, subscribers and authorised users (“Users”), for small-scale personal, non-commercial use provided that all copyright, trade and service marks and other proprietary notices are maintained. By accessing, sharing, receiving or otherwise using the Springer Nature journal content you agree to these terms of use (“Terms”). For these purposes, Springer Nature considers academic use (by researchers and students) to be non-commercial.
These Terms are supplementary and will apply in addition to any applicable website terms and conditions, a relevant site licence or a personal subscription. These Terms will prevail over any conflict or ambiguity with regards to the relevant terms, a site licence or a personal subscription (to the extent of the conflict or ambiguity only). For Creative Commons-licensed articles, the terms of the Creative Commons license used will apply.
We collect and use personal data to provide access to the Springer Nature journal content. We may also use these personal data internally within ResearchGate and Springer Nature and as agreed share it, in an anonymised way, for purposes of tracking, analysis and reporting. We will not otherwise disclose your personal data outside the ResearchGate or the Springer Nature group of companies unless we have your permission as detailed in the Privacy Policy.
While Users may use the Springer Nature journal content for small scale, personal non-commercial use, it is important to note that Users may not:

1. use such content for the purpose of providing other users with access on a regular or large scale basis or as a means to circumvent access control;
2. use such content where to do so would be considered a criminal or statutory offence in any jurisdiction, or gives rise to civil liability, or is otherwise unlawful;
3. falsely or misleadingly imply or suggest endorsement, approval , sponsorship, or association unless explicitly agreed to by Springer Nature in writing;
4. use bots or other automated methods to access the content or redirect messages
5. override any security feature or exclusionary protocol; or
6. share the content in order to create substitute for Springer Nature products or services or a systematic database of Springer Nature journal content.

In line with the restriction against commercial use, Springer Nature does not permit the creation of a product or service that creates revenue, royalties, rent or income from our content or its inclusion as part of a paid for service or for other commercial gain. Springer Nature journal content cannot be used for inter-library loans and librarians may not upload Springer Nature journal content on a large scale into their, or any other, institutional repository.
These terms of use are reviewed regularly and may be amended at any time. Springer Nature is not obligated to publish any information or content on this website and may remove it or features or functionality at our sole discretion, at any time with or without notice. Springer Nature may revoke this licence to you at any time and remove access to any copies of the Springer Nature journal content which have been saved.
To the fullest extent permitted by law, Springer Nature makes no warranties, representations or guarantees to Users, either express or implied with respect to the Springer nature journal content and all parties disclaim and waive any implied warranties or warranties imposed by law, including merchantability or fitness for any particular purpose.
Please note that these rights do not automatically extend to content, data or other material published by Springer Nature that may be licensed from third parties.
If you would like to use or distribute our Springer Nature journal content to a wider audience or on a regular basis or in any other manner not expressly permitted by these Terms, please contact Springer Nature at

onlineservice@springernature.com